Nonlinear System Identification Using Exponential Swept-Sine Signal

Antonín Novák, Laurent Simon, *Member, IEEE*, František Kadlec, and Pierrick Lotton

***Abstract*—In this paper, we propose a method for nonlinear system (NLS) identification using a swept-sine input signal and based on nonlinear convolution. The method uses a nonlinear model, namely, the nonparametric generalized polynomial Hammerstein model made of power series associated with linear filters. Simulation results show that the method identifies the nonlinear model of the system under test and estimates the linear filters of the unknown NLS. The method has also been tested on a real-world system: an audio limiter. Once the nonlinear model of the limiter is identified, a test signal can be regenerated to compare the outputs of both the real-world system and its nonlinear model. The results show good agreement between both model-based and real-world system outputs.**

***Index Terms*—Analysis, generalized polynomial Hammerstein model, identification, nonlinear convolution, nonlinear system (NLS), swept-sine.**

I. Introduction

THE theory of linear time-invariant (LTI) systems has been extensively studied over decades [1], [2], and the estimation of any unknown LTI system, knowing both the input and output of the system, is a solved problem. The fundamental idea of the theory states that any LTI system can be characterized entirely by its impulse response in the time domain or by its frequency response function in the frequency domain. Nevertheless, almost all real-world devices exhibit more or less nonlinear behavior. In the case of very weak nonlinearities, a linear approximation can be used. If the nonlinearities are stronger, the linear approximation fails, and the system has to be described using a nonlinear model. Such nonlinear models are available in the literature, e.g., the Volterra model [3], the neural network model [4], the multiple-input–single-output (MISO) model [5], the nonlinear autoregressive moving average with exogenous inputs model [6], [7], the hybrid genetic algorithm [8], extended Kalman filtering [9], and particle filtering [10].

Manuscript received July 21, 2008; revised August 14, 2009; accepted August 14, 2009. Date of publication October 30, 2009; date of current version July 14, 2010. This work was supported in part by the Ministry of Education of Czech Republic under the research program "Research in the Area of the Prospective Information and Navigation Technologies" under Contract MSM6840770014 and in part by the French Embassy in Prague within the framework of the program "Cotutelle de thèse." The Associate Editor coordinating the review process for this paper was Dr. Jesús Ureña.

A. Novák is with Laboratoire d'Acoustique de l'Université du Maine, Unite Mixte de Recherche-Centre National de la Recherche Scientifique (UMR-CNRS) 6613, 72085 Le Mans, France, and also with the Faculty of Electrical Engineering, Czech Technical University, Prague 166 27, Czech Republic (e-mail: ant.novak@gmail.com).

L. Simon and P. Lotton are with Laboratoire d'Acoustique de l'Université du Maine, UMR-CNRS 6613, 72085 Le Mans, France.

F. Kadlec is with Faculty of Electrical Engineering, Czech Technical University, Prague 166 27, Czech Republic.

Digital Object Identifier 10.1109/TIM.2009.2031836

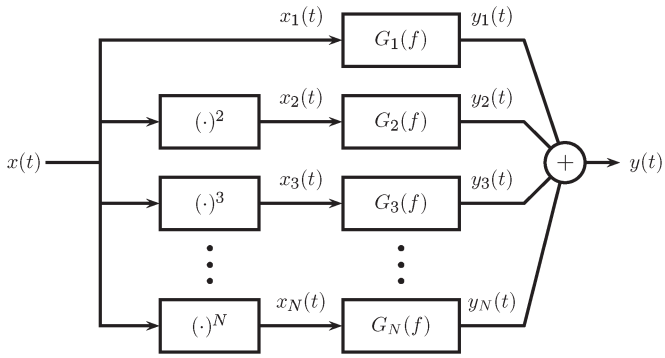

Fig. 1. Generalized polynomial Hammerstein model (power series nonlinear model).

All these models involve parameters or kernels that have to be estimated. If a theoretical physical model of the nonlinear system (NLS) under test is available, the global nonlinear behavior of the system is known, and the method to be carried out consists of the estimation of the unknown parameters of the NLS. If no prior knowledge of the NLS is available, an identification procedure has to be involved. This procedure is based on the analysis of the signal produced at the output of the system under test when exciting the system by a given and controlled input signal. Different input signals can be used, depending on the method chosen for the estimation, such as sine wave excitation, multitone excitation [11]–[13], random noise excitation [5], and pseudorandom signals [14], [15].

Regarding the basics of the NLS theory, when a pure sine-wave input signal $x(t) = A_1 \cos(2\pi f_1 t + \phi_1)$ passes through an NLS, higher harmonics appear at the output of the system as multiples of input frequency, according to $y(t) = \sum_n B_n \cos(2\pi n f_1 t + \phi_n)$. The characteristics (i.e., amplitude B_n and phase ϕ_n) of all higher order components may, furthermore, be frequency and input amplitude dependent, in the sense that $\forall n \;\; B_n \equiv B_n(A_1, f_1), \;\; \phi_n \equiv \phi_n(A_1, f_1)$. The complete identification procedure consequently needs to estimate the amplitude B_n and phase ϕ_n as functions of input amplitude and frequency. Nonlinear models, including frequency dependence, are, e.g., the Wiener model, the Hammerstein model, and the Wiener–Hammerstein model [15].

A nonparametric generalized polynomial Hammerstein model [15] of order N is considered here, as illustrated in Fig. 1. The model is made up of N parallel branches, with each branch consisting of a linear filter $G_n(f)$ preceded by an nth power static nonlinear function. Giving both the input and output signals $x(t)$ and $y(t)$, the problem of identifying the generalized polynomial Hammerstein model consists then of estimating the unknown linear filters $G_n(f)$, $n \in [1, N]$.

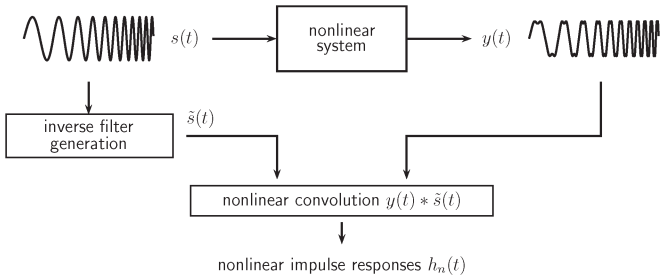

Fig. 2. Block diagram of the nonlinear convolution process in NLS identification.

In this paper, we propose a new method for identifying the generalized polynomial Hammerstein model based on an input exponential swept-sine signal, allowing a one-path estimation of the unknown linear filters. This paper is organized as follows. In Section II, we review the basics of the nonlinear convolution first proposed in [16] and [17], and we recall the properties of asymptotic signals. In Section III, we define the swept-sine input signal, and we detail how to design this input signal for the purpose of NLS identification. In Section IV, we define the associated inverse filter, and we show how to estimate the linear filters of the model. In Section V, we show the results of numerical experiments and real NLS identification (audio limiter). In Section VI, the proposed method is compared with other methods based on dedicated models [25], such as the Hammerstein or Wiener models. Finally, conclusions are noted in Section VII.

II. Basics of the Method

The method presented in this paper is partly based on the nonlinear convolution method presented in [17]. The method uses a swept-sine signal (also called a chirp), exhibiting an exponential instantaneous frequency as the excitation signal, and allows the characterization of an NLS in terms of harmonic distortion at several orders. This nonlinear convolution method and the basic theory of instantaneous frequency and complex signal are reviewed in this section.

A. Nonlinear Convolution

The block diagram of the method is shown in Fig. 2. First, an exponential swept-sine signal $s(t)$ is generated and used as the input signal of the NLS under test. The distorted output signal $y(t)$ is recorded for being used for the so-called nonlinear convolution [17]. Next, the signal, denoted as $\tilde{s}(t)$, is derived from the input signal $s(t)$ as its time-reversed replica with amplitude modulation such that the convolution between $s(t)$ and $\tilde{s}(t)$ gives a Dirac delta function $\delta(t)$. The signal $\tilde{s}(t)$ is called "inverse filter" [16], [17]. Then, the convolution between the output signal $y(t)$ and the inverse filter $\tilde{s}(t)$ is performed. The result of this convolution can be expressed as

$$y(t) * \tilde{s}(t) = \sum_{m=1}^{\infty} h_m(t + \Delta t_m) \tag{1}$$

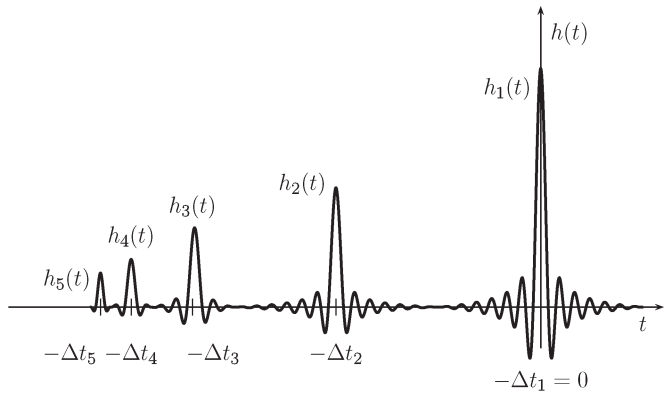

Fig. 3. Result of the nonlinear convolution process $y(t) * \tilde{s}(t)$ in the form of a set of higher order $h_m(t)$.

where $h_m(t)$ represents the higher order impulse responses, and Δt_m represents the time lag between the first (linear) and the mth impulse response. Since the nonlinear impulse response consists of a set of higher order impulse responses that are time shifted, each partial impulse response can be separated from each other, as illustrated in Fig. 3. This procedure is developed in [16].

The set of higher order $h_m(t)$ can also be expressed in the frequency domain. The frequency response functions of higher order $h_m(t)$ are then their Fourier transforms, i.e.,

$$H_m(f) = \mathbf{FT}\left[h_m(t)\right]. \tag{2}$$

The frequency responses $H_m(f)$ represent the frequency dependence of higher order components. The frequency response $H_1(f)$ is consequently the response corresponding to the linear part of the system. Similarly, the frequency response $H_m(f)$ $(m > 1)$ may be regarded as the system frequency response, when considering only the effect of the input frequency f on the mth harmonic frequency mf of the output. The relation between partial frequency responses $H_m(f)$ and linear filters $G_n(f)$ is detailed in Section IV.

B. Instantaneous Frequency and Complex Signal

A swept-sine signal, or chirp, is a signal in which the instantaneous frequency increases with time and can generally be defined as

$$s(t) = a(t)\sin\left(\varphi(t)\right). \tag{3}$$

The analytic signal of the signal $s(t)$ is

$$z_s(t) = s(t) + jH\left[s(t)\right] = a_s(t)e^{j\varphi_s(t)} \tag{4}$$

where $H[\,]$ is the Hilbert transform, and $a_s(t)$ and $\varphi_s(t)$ are unambiguously defined as the amplitude and the phase of $z_s(t)$. The spectrum $Z_s(f)$ of the signal $z_s(t)$ can be written in terms of amplitude and phase as

$$Z_s(f) = B_s(f)e^{j\Psi_s(f)}. \tag{5}$$

The instantaneous frequency $f_i(t)$ and the group delay $t_f(t)$ are then defined as

$$f_i(t) = \frac{1}{2\pi}\frac{d\varphi_s(t)}{dt} \tag{6}$$

$$t_f(f) = -\frac{1}{2\pi}\frac{d\Psi_s(f)}{df}. \tag{7}$$

Equations (6) and (7) define two curves in the time–frequency planes, which, for strictly monotonic chirps or so-called asymptotic signals [18], [19], may be regarded as the inverse of each other. In such conditions of asymptotic signal, if one of these functions is known, the other one can then easily be calculated. Furthermore, we can write the following equalities: $t \equiv t_f \equiv t_f(f)$ and $f \equiv f_i \equiv f_i(t)$.

These properties allow us to know the spectra of the signal $z_s(t)$ with no need of calculating its Fourier transform. The amplitude $a_s(t)$ and the phase $\varphi_s(t)$ in the time domain are related to the amplitude $B_s(f)$ and the phase $\Psi_s(f)$ in the frequency domain, for $f > 0$, as [20]

$$B_s(f) = \frac{a_s(t_f)}{\sqrt{\frac{1}{2\pi}\left|\varphi_s''(t_f)\right|}} \tag{8}$$

$$\Psi_s(f) = \varphi_s(t_f) - 2\pi f t_f + \frac{\pi}{4}\text{sign}\left(\frac{df_i(t_f)}{dt_f}\right). \tag{9}$$

III. Input Signal and Inverse Filter: Design and Properties

In this section, we detail how the input signal used for the identification of the NLS under test is designed. First, the input signal is defined as an exponential swept-sine signal as used in [16] and [17]. Then, a redesign of this input signal is proposed for the specific purpose of estimation of the linear filters of the nonparametric generalized polynomial Hammerstein model. Both time- and frequency-domain properties of this redesigned signal are also examined.

A. Input Signal Design

The input signal used for the identification is an exponential swept-sine signal, i.e., a signal exhibiting an instantaneous frequency that increases exponentially with time. Such a signal is also called an exponential chirp and is defined as

$$s(t) = \sin\left[2\pi f_1 \int_0^t \exp\left(\frac{t'}{L}\right)dt'\right]$$

$$= \sin\left\{2\pi f_1 L\left[\exp\left(\frac{t}{L}\right) - 1\right]\right\} \tag{10}$$

where f_1 is the start frequency at $t = 0$, and L is the rate of exponential increase in frequency. The parameter L depends on the time length T and the stop frequency f_2 of the swept-sine signal. The signal $s(t)$ defined in (10) can also be expressed as in (3), with a constant amplitude envelope, i.e., $a(t) = 1$, and the instantaneous phase

$$\varphi(t) = 2\pi f_1 L\left[\exp\left(\frac{t}{L}\right) - 1\right]. \tag{11}$$

The instantaneous frequency, which is defined in (6), is

$$f_i(t) = f_1 \exp\left(\frac{t}{L}\right). \tag{12}$$

The group delay t_f is then the inverse function of the instantaneous frequency f_i and is given by

$$t_f(f) = L\,\log\left(\frac{f_i}{f_1}\right). \tag{13}$$

The time length T of the signal $s(t)$ can then be consequently expressed as the time between two particular instantaneous frequencies f_1 (start frequency) and f_2 (stop frequency), i.e.,

$$T = L\,\log\left(\frac{f_2}{f_1}\right) \tag{14}$$

and thus, the coefficient L is defined as

$$L = \frac{T}{\log\left(\frac{f_2}{f_1}\right)}. \tag{15}$$

This definition of the swept-sine signal parameters is similar to the one used in [16], [17], and [21] for analysis of audio equipment nonlinearities. Nevertheless, for the nonlinear model estimation, this definition may lead to problems due to nonsynchronization of the phases of the higher order impulse responses. For that reason, the following procedure is proposed to redesign the exponential swept-sine signal. First, let Δt_m be the time lag, for which the instantaneous frequency $f_i(\Delta t_m)$ is given by

$$f_i(\Delta t_m) = m f_1 \tag{16}$$

for $m \in \mathbb{N} - \{0\}$. Using (13), it is then possible to write

$$\Delta t_m = L\,\log(m) \tag{17}$$

and the instantaneous phase at the time lag Δt_m is given by

$$\varphi(\Delta t_m) = 2\pi f_1 L(m-1). \tag{18}$$

Second, as depicted in Fig. 4, the swept-sine signal $s(t)$ at a particular time lag Δt_m is designed to be equal to zero, i.e., $s(\Delta t_m) = 0$, with the additional constraint of a positive first derivative, i.e., $s'(\Delta t_m) > 0$. These conditions consequently yield to

$$\varphi(\Delta t_m) = 2k\pi \tag{19}$$

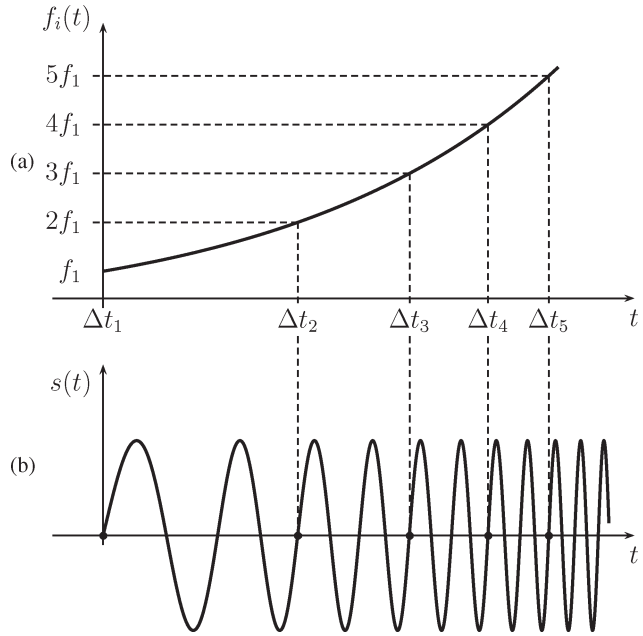

Fig. 4. (a) Swept-sine signal $s(t)$ in the time domain, with (b) the time length chosen according to instantaneous frequency $f_i(t)$.

where $k \in \mathbb{Z}$. Thus, from (18) and (19), we get

$$f_1 L(m-1) = k. \tag{20}$$

A sufficient condition to solve (20) is then

$$f_1 L \in \mathbb{Z}. \tag{21}$$

Using (15) and this condition, we write

$$L = \frac{1}{f_1} Round\left(\frac{\hat{T} f_1}{\log\left(\frac{f_2}{f_1}\right)}\right) \tag{22}$$

where $\hat{T}$ is an approximate time length of the signal $s(t)$, and $Round$ represents rounding toward nearest integer.

The redesigned exponential swept-sine signal can then be generated using (10) and (22). The parameters that define the input signal $s(t)$ are the start and stop frequencies f_1 and f_2 and the approximate time length $\hat{T}$.

B. Time-Domain Properties of the Input Signal

The signal $s(t)$ defined above and satisfying the conditions depicted in Fig. 4, furthermore, has the following property. Consider a signal $s_2(t)$ with an instantaneous frequency that is equal to twice the instantaneous frequency of the signal $s(t)$. The relation between both signals is then

$$s_2(t) = s(t + \Delta t_2). \tag{23}$$

This condition may be extended for any $m \in \mathbb{N} - \{0\}$, as

$$s_m(t) = s(t + \Delta t_m). \tag{24}$$

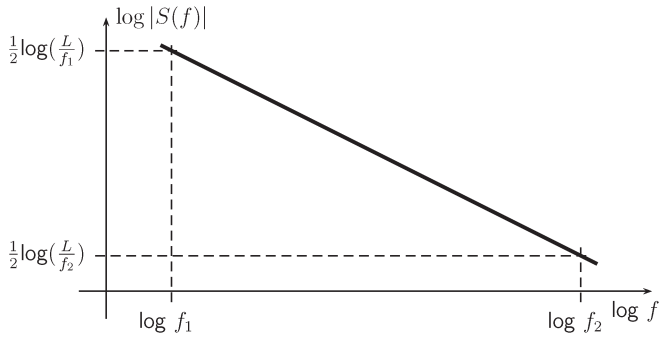

Fig. 5. Amplitude of the Fourier transform of the exponential swept-sine signal.

C. Frequency-Domain Properties of the Input Signal

To derive the amplitude spectrum $B_s(f)$ of the analytic swept-sine signal $z_s(t)$, we use (8). The second-order derivative of the phase $\varphi_s(t)$ is expressed, using (11) and (13), as

$$\varphi_s''(t) = \varphi''(t) = \frac{2\pi f_1}{L} \exp\left(\frac{t}{L}\right) = \frac{2\pi f_i(t)}{L}. \tag{25}$$

Using (8) and (25) and the equivalence $f \equiv f_i$, the amplitude spectrum, for $f > 0$, can be written as

$$B_s(f) = \sqrt{\frac{L}{f}} \tag{26}$$

as depicted in Fig. 5.

D. Inverse Filter

We consider here the analytic signal of the inverse filter $\tilde{s}(t)$ as

$$z_{\tilde{s}}(t) = \tilde{s}(t) + jH\left[\tilde{s}(t)\right] \tag{27}$$

and the Fourier transform $Z_{\tilde{s}}(f)$ of the analytic signal $z_{\tilde{s}}(t)$. The inverse filter $\tilde{s}(t)$ convolved with the swept-sine signal $s(t)$ gives, theoretically, the Dirac function $\delta(t)$ as well as their analytic signals, and thus, we can write

$$Z_{\tilde{s}}(f) = \frac{1}{Z_s(f)}. \tag{28}$$

To express the analytic signal of the inverse filter $z_{\tilde{s}}(t)$, we first derive the relation between magnitudes and phases of both Fourier transforms as

$$Z_{\tilde{s}}(f) = \frac{1}{B_s(f) e^{j\Psi_s(f)}} = \frac{1}{B_s(f)} e^{-j\Psi_s(f)} \tag{29}$$

and thus

$$B_{\tilde{s}}(f) = |Z_{\tilde{s}}(f)| = \frac{1}{B_s(f)} \tag{30}$$

$$\Psi_{\tilde{s}}(f) = -\Psi_s(f). \tag{31}$$

For asymptotic signal $z_s(t)$, the analytic inverse filter $z_{\tilde{s}}(t)$ is, consequently, also an asymptotic signal, i.e.,

$$z_{\tilde{s}}(t) = a_{\tilde{s}}(t)e^{j\tilde{\varphi}_s(t)}. \tag{32}$$

Then, we derive the phase $\tilde{\varphi}_s(t)$ from the expression of $\tilde{t}_f(f)$. Using (7) and (31), we get

$$\tilde{t}_f(f) = -\frac{1}{2\pi}\frac{d\Psi_{\tilde{s}}(f)}{df} = \frac{1}{2\pi}\frac{d\Psi_s(f)}{df}. \tag{33}$$

Consequently, we get

$$\tilde{t}_f(f) = -t_f(f) \tag{34}$$

$$\tilde{\varphi}_s(t) = \varphi_s(-t). \tag{35}$$

We use (8) to derive the amplitude $a_{\tilde{s}}(t)$ of the inverse filter as follows:

$$B_{\tilde{s}}(f) = \frac{a_{\tilde{s}}(\tilde{t}_f)}{\sqrt{\frac{1}{2\pi}\left|\tilde{\varphi}_s''(\tilde{t}_f)\right|}}. \tag{36}$$

As $\tilde{\varphi}_s''(\tilde{t}_f) = \varphi_s''(t_f)$ [from (34) and (35)], we can substitute from (25)

$$B_{\tilde{s}}(f) = \frac{a_{\tilde{s}}(\tilde{t}_f)}{\sqrt{\frac{f}{L}}}. \tag{37}$$

Now, from (26), (30), and (37) we can write

$$a_{\tilde{s}}(\tilde{t}_f) = \frac{f_i}{L}. \tag{38}$$

Using (12), the envelope $a_{\tilde{s}}(t)$ is given by

$$a_{\tilde{s}}(t) = \frac{f_1}{L}\exp\left(-\frac{t}{L}\right) \tag{39}$$

and the analytic inverse filter is finally expressed as

$$z_{\tilde{s}}(t) = \frac{f_1}{L}\exp\left(-\frac{t}{L}\right)e^{j(\varphi_s(-t))} \tag{40}$$

i.e., in shorten form, we have

$$z_{\tilde{s}}(t) = \frac{f_1}{L}\exp\left(-\frac{t}{L}\right)z_s(-t). \tag{41}$$

The inverse filter $\tilde{s}(t)$ is then

$$\tilde{s}(t) = \frac{f_1}{L}\exp\left(-\frac{t}{L}\right)s(-t). \tag{42}$$

IV. Principles of the Method of Identification

In Section III, the input signal $s(t)$ and the inverse filter $\tilde{s}(t)$ have been defined to be used for identification of the NLS under test. This section focuses on the relation between partial frequency responses $H_m(f)$ and linear filters $G_n(f)$ in the frequency domain.

As the impulse responses $h_m(t)$ and $g_n(t)$, defined as the inverse Fourier transform of $H_m(f)$ and $G_n(f)$, respectively, are supposed to be real functions, it follows from the Hermitian properties of $H_m(f)$ and $G_n(f)$ that only the half frequency area $f > 0$ is considered in the following.

Given the partial frequency responses $H_m(f)$ defined by (2), the frequency response of the linear filters $G_n(f)$ of the power series nonlinear model can be derived analytically using the trigonometric power formulas, defined as [22]

$$(\sin x)^{2l+1} = \frac{(-1)^l}{4^l}\sum_{k=0}^{l}(-1)^k\binom{2l+1}{k}\sin\left[(2l+1-2k)x\right] \tag{43}$$

$\forall\, l \in \mathbb{N}$ and

$$(\sin x)^{2l} = \frac{(-1)^l}{2^{2l-1}}\sum_{k=0}^{l-1}(-1)^k\binom{2l}{k}\cos\left[2(l-k)x\right] + \frac{1}{2^{2l}}\binom{2l}{l} \tag{44}$$

$\forall\, l \in \mathbb{N} - \{0\}$.

Regarding the Fourier transform of (43) and (44), and noting FT_p the result of the Fourier transform only for positive frequencies, we can write

$$\mathrm{FT}_p\left\{(\sin x)^{2l+1}\right\} = \frac{(-1)^l}{4^l}\sum_{k=0}^{l}(-1)^k\binom{2l+1}{k} \times \mathrm{FT}_p\left\{\sin\left[(2l+1-2k)x\right]\right\} \tag{45}$$

$\forall\, l \in \mathbb{N}$ and

$$\mathrm{FT}_p\left\{(\sin x)^{2l}\right\} = j\frac{(-1)^l}{2^{2l-1}}\sum_{k=0}^{l-1}(-1)^k\binom{2l}{k} \times \mathrm{FT}_p\left\{\sin\left[2(l-k)x\right]\right\} + \frac{1}{2^{2l}}\binom{2l}{l} \tag{46}$$

$\forall\, l \in \mathbb{N} - \{0\}$.

These formulas give in the Fourier domain the relation between the higher order harmonic $\sin(lx)$ and the lth power of the harmonic signal $\sin^l(x)$, for $l \in \mathbb{N}$. Considering a harmonic input signal of frequency $f_0 > 0$, the values of the frequency responses $H_m(lf_0)$ and the values of the frequency responses of the linear filters $G_n(lf_0)$ are related in the same way as in (43) and (44).

The trigonometric formulas in the frequency domain can then be rewritten into the matrix form (47), where the matrices $\mathbf{A}$ and $\mathbf{B}$ represent the coefficients in (45) and (46), i.e.,

$$\begin{pmatrix} \mathrm{FT}_p\{\sin x\} \\ \mathrm{FT}_p\{\sin^2 x\} \\ \mathrm{FT}_p\{\sin^3 x\} \\ \vdots \end{pmatrix} = \mathbf{A}\begin{pmatrix} \mathrm{FT}_p\{\sin x\} \\ \mathrm{FT}_p\{\sin 2x\} \\ \mathrm{FT}_p\{\sin 3x\} \\ \vdots \end{pmatrix} + \mathbf{B}. \tag{47}$$

The matrix $\mathbf{A}$ is defined, according to (45) and (46), as

$$A_{n,m} = \begin{cases} \frac{(-1)^{2n+\frac{1-m}{2}}}{2^{n-1}}\binom{n}{\frac{n-m}{2}}, & \text{for } n \geq m \text{ and} \\ & (n+m) \text{ is even} \\ 0, & \text{else.} \end{cases} \tag{48}$$

The matrix $\mathbf{B}$ is a one-column matrix and represents the constant values of the even power series. These values are only

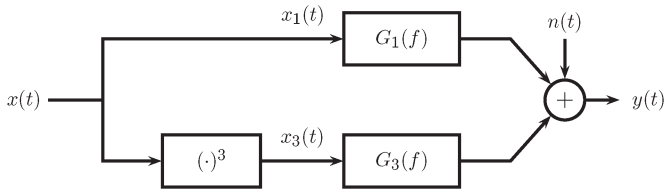

Fig. 6. Simulated NLS with memory.

linked to the mean value of the output signal. The relation between the partial frequency response $H_m(f_0)$, for $f_0 > 0$, and the linear filters $G_n(f_0)$ from the power series nonlinear model is given using the coefficients of the matrix $\mathbf{A}$. Each partial frequency response $H_m(f_0)$, or mth harmonic, can be expressed as a sum of the mth harmonics of all the nth powers weighted by the linear filters $G_n(f_0)$. The coefficients of the mth harmonics of the nth power are $A(n,m)$ and thus

$$H_m(f_0) = \sum_{n=1}^{N} A_{n,m} G_n(f_0). \tag{49}$$

Finally, the linear transformation between $H_m(f_0)$ and $G_n(f_0)$, for $f_0 > 0$, can generally be expressed in matrix form as

$$\begin{pmatrix} G_1(f_0) \\ G_2(f_0) \\ G_3(f_0) \\ \vdots \end{pmatrix} = (\mathbf{A}^T)^{-1} \begin{pmatrix} H_1(f_0) \\ H_2(f_0) \\ H_3(f_0) \\ \vdots \end{pmatrix} \tag{50}$$

where $\mathbf{A}^T$ denotes the transpose of $\mathbf{A}$.

V. Results

A. Simulation of an NLS With Memory

To illustrate the method, a simulated NLS with memory is identified. This NLS consists of two nonlinear branches with linear and cubic parts, each of them followed by a linear filter (Fig. 6). To simulate real-world conditions, a white Gaussian noise $n(t)$ is added to the output signal. Both filters are digital Butterworth filters. The filter $G_1(f)$ used in the linear branch is a tenth-order high-pass filter, with a cutoff frequency of 500 Hz, and the filter $G_3(f)$ used in the cubic branch is a tenth-order low-pass filter, with a cutoff frequency of 1 kHz. The simulation is performed using a sampling frequency $f_s =$ 12 kHz. The excitation signal used for the identification is a swept-sine signal, as defined in Section III, with the following parameters: $f_1 = 20$ Hz; $f_2 = 2000$ Hz; and $\hat{T} = 5$ s. The maximum frequency f_2 has been chosen to avoid any aliasing [23], [24]. The order of the model is set to $N = 3$. Once the response of the NLS under test to this excitation signal is known, the nonlinear convolution described in Section IV is performed, and the linear filters of the nonlinear model are estimated.

The estimated frequency responses (modulus and phases) of filters $\hat{G}_1(f)$ and $\hat{G}_2(f)$ are, respectively, given in Figs. 7 and 8 and compared to the theoretical ones (Figs. 9 and 10), with a signal-to-noise ratio (SNR) equal to 30 dB. In the frequency ranges of the swept-sine input signal ($f_1 = 20$ Hz, $f_2 = 2$ kHz), both estimated filters, i.e., the high-pass filter

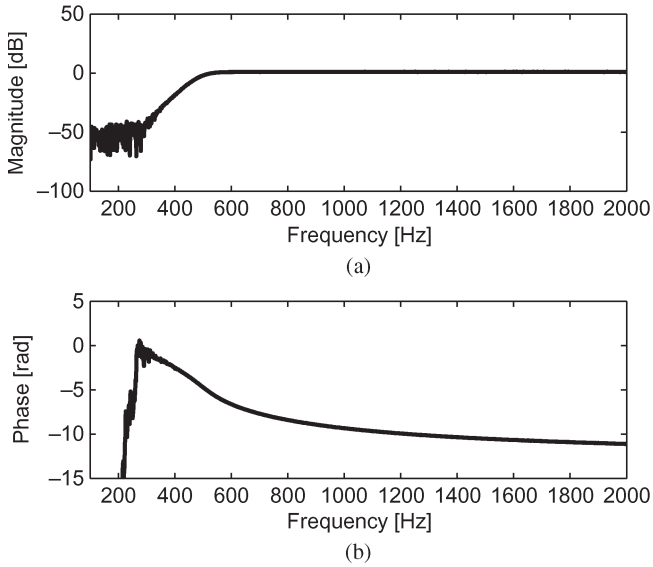

Fig. 7. Estimated frequency response of the filter $\hat{G}_1(f)$ from the linear part of the tested system. (a) Modulus. (b) Phase.

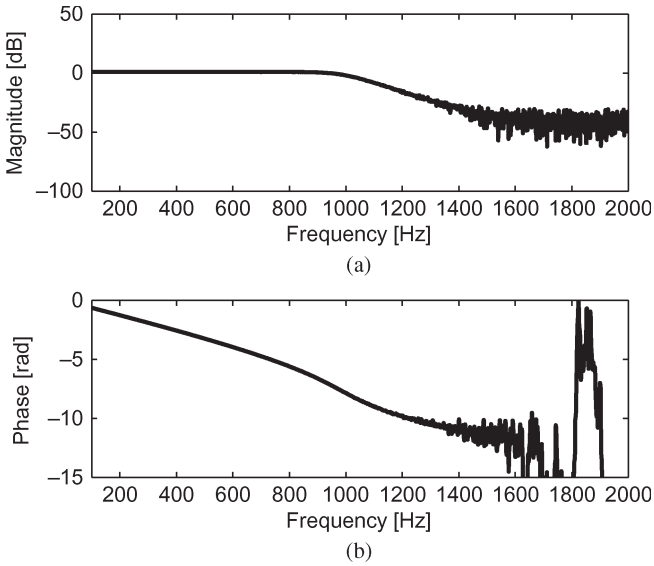

Fig. 8. Estimated frequency response of the filter $\hat{G}_3(f)$ from the nonlinear part of the tested system. (a) Modulus. (b) Phase.

(500–2000 Hz) and the low-pass filter (50–1000 Hz), match in amplitude and phase with the theoretical characteristics.

To test the robustness of the identification method, the simulation has also been performed for several levels of additive noise $n(t)$. The mean square error (MSE) of the estimated filters depends, indeed, on the SNR. The MSE is calculated as the mean square of the modulus of the complex difference between the estimated and real filters in the frequency range $[f_1 =$ 20 Hz, $f_2 = 2$ kHz]. No synchronous averaging is performed.

The robustness of the method is illustrated in Fig. 11. As expected, the MSE is made up of the following two contributions: 1) the error caused by the additive noise $n(t)$ and 2) the model error [25]. The proposed method estimates the linear filters of the model with an error less than $\simeq 10^{-2}$, even for the lowest simulated SNR. For SNRs higher than 50 dB, the MSE remains constant, due to the model error, at a value close to $\simeq 10^{-6}$.

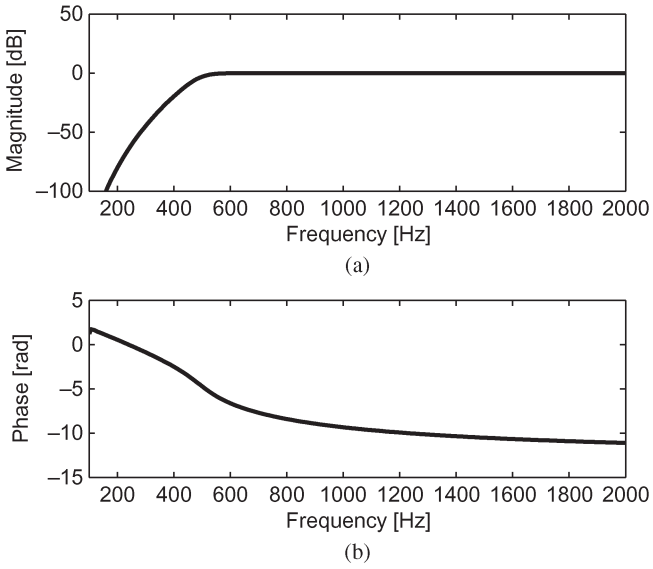

Fig. 9. Theoretical frequency response of the filter $G_1(f)$ from the linear part of the tested system. (a) Modulus. (b) Phase.

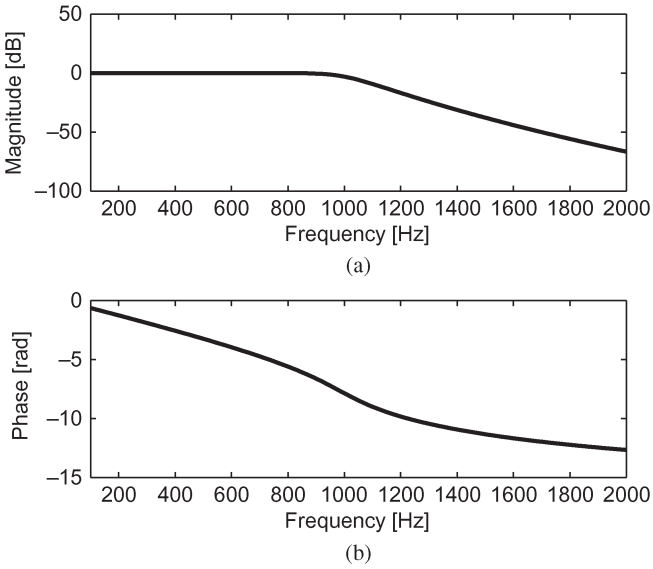

Fig. 10. Theoretical frequency response of the filter $G_3(f)$ from the nonlinear part of the tested system. (a) Modulus. (b) Phase.

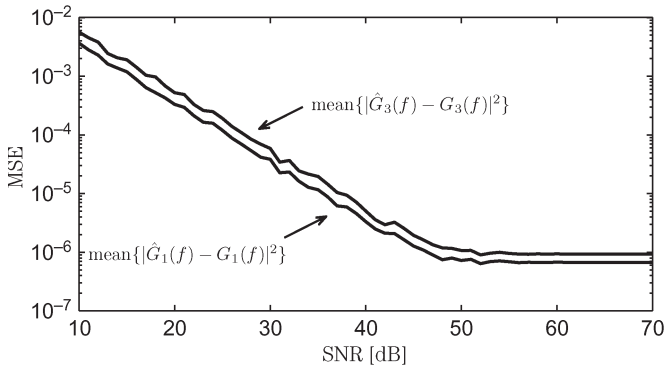

Fig. 11. Dependence of the MSE of the estimated filters $\hat{G}_1(f)$ and $\hat{G}_3(f)$ on SNR.

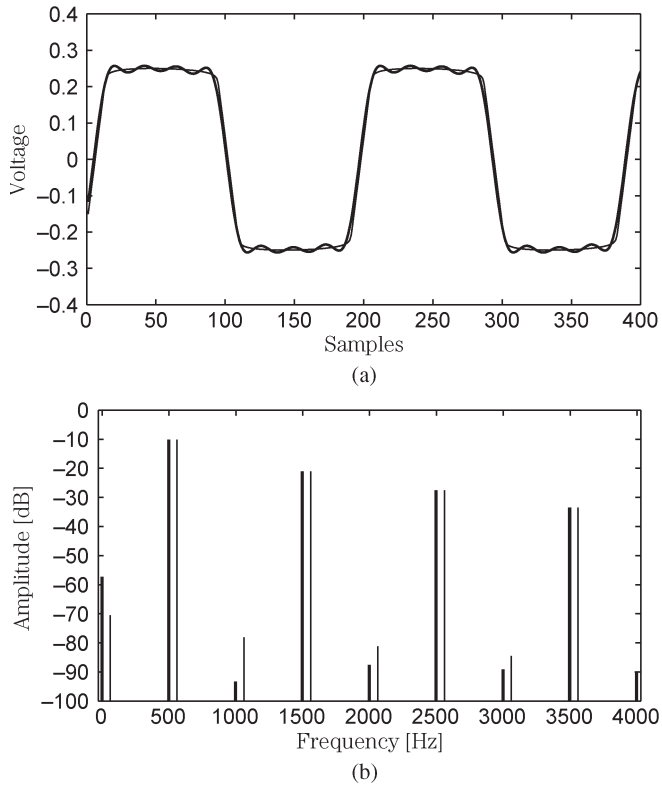

Fig. 12. Comparison of the real-world (thin) and regenerated (bold) responses to the sine wave, with $f = 500$ Hz and $A = 1$ V. (a) Waveforms. (b) Spectra.

B. Identification of a Real NLS

In this section, a real-world NLS is selected for testing the proposed method. The system under test is the limiter part of a *dbx 266XL* compressor limiter gate [26]. The limiter is an NLS producing highly distorted output waveforms. The clipping level of the limiter is set to 0.25 V.

The measurements are performed using the swept-sine excitation signal, with amplitude $A = 1$ V, frequencies $f_1 = 10$ Hz and $f_2 = 5$ kHz, and approximate time duration $\hat{T} = 6$ s. The sampling frequency is $f_s = 96$ kHz, and the order of the model is $N = 8$.

To verify the accuracy of the estimated model, a signal $x(t)$ is generated and used as the input signal of both the model and the real-world limiter. The responses $y_r(t)$ of the model and $y(t)$ of the limiter are then compared in both the time and frequency domains. Three comparisons, corresponding to three different input signals, are performed. As an objective criterion, a mean square residual error between regenerated and measured output waveforms is measured for all the three cases.

First, a sine-wave input signal is generated with frequency $f_0 = 500$ Hz and amplitude $A_0 = 1$ V. Both regenerated and real-world system outputs are then compared in Fig. 12. For the sake of clarity, the output of the real limiter in the frequency domain is shifted to the right. On one hand, the output of the real-world system consists of numerous higher harmonics. On the other hand, the model is truncated to the eighth order. Consequently, the regenerated output signal cannot contain more than eight higher harmonics and then exhibits well-known oscillations, known as the Gibbs phenomenon. Nevertheless, the regenerated output signal fits in with MSE $= 2.3 \cdot 10^{-4}$.

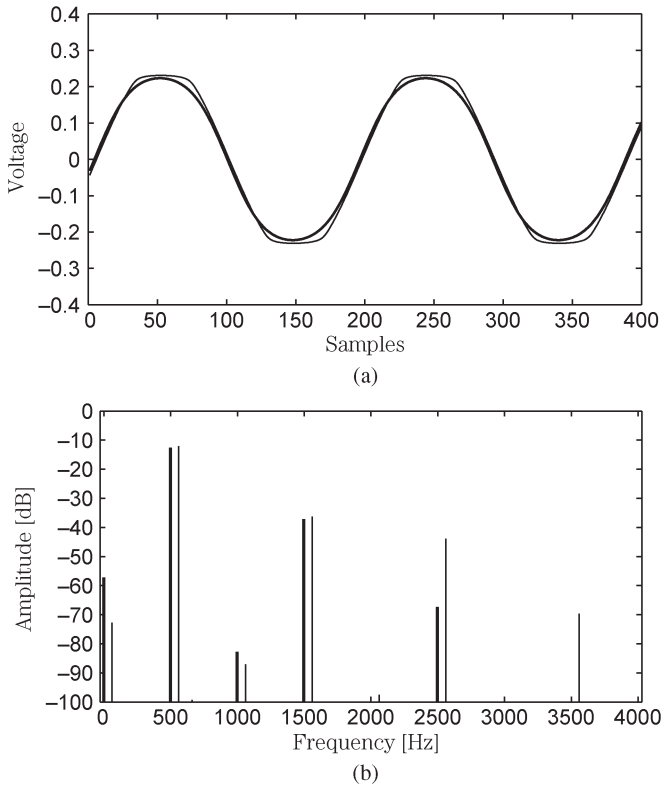

Fig. 13. Comparison of the real-world (thin) and regenerated (bold) responses to the sine wave, with $f = 500$ Hz and $A = 0.3$ V. (a) Waveforms. (b) Spectra.

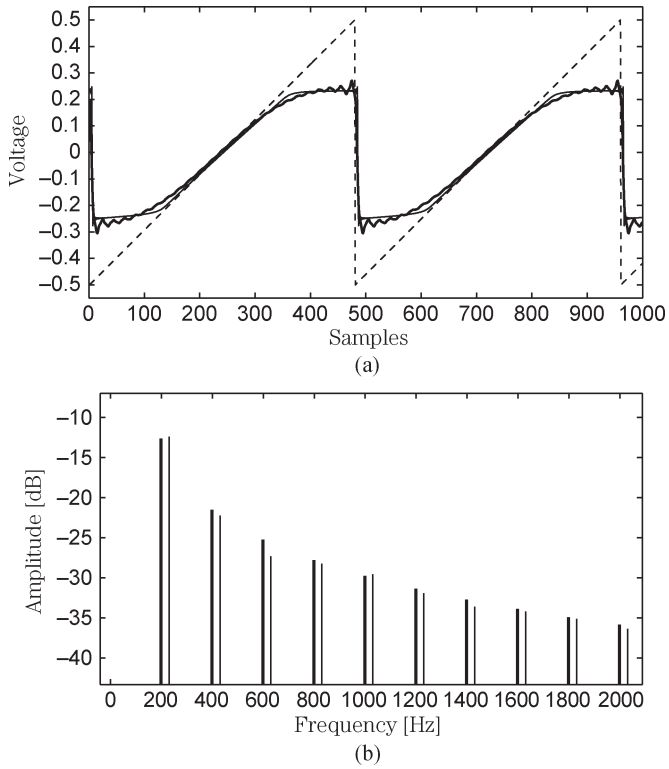

Fig. 14. Comparison of the real-world (thin) and regenerated (bold) responses to the sawtooth input signal (dashed). (a) Waveforms. (b) Spectra.

Second, the input signal is a sine wave with the same frequency ($f_0 = 500$ Hz) but with a lower amplitude ($A_0 = 0.3$ V). Both regenerated and real-world systems are compared in Fig. 13, which shows that the nonlinear model fits in also well for a lower input signal, even if the fourth odd component is poorly estimated, suggesting a possible input–output law, depending on the amplitude of the input signal. As for the previous case, MSE $= 2.3 \cdot 10^{-4}$.

Finally, a sawtooth input signal is used as the input signal, and the measured and regenerated output signals are compared. The sawtooth signal is chosen to exhibit a period of 480 samples, equivalent to a frequency of 200 Hz, for a data rate $f_s = 96$ kHz. The results are depicted in Fig. 14. The regenerated and measured output waveforms are very similar, even if the regenerated one exhibits Gibbs oscillations. The MSE between regenerated and measured output waveforms is MSE $= 6.6 \cdot 10^{-4}$. This confirms that the method is accurate enough for regenerating complex output waveforms.

VI. Comparison With Existing Methods

There is a wide variety of methods in the literature of NLS identification. On one hand, methods based on Wiener, Hammerstein, MISO, or block-oriented models may be considered as methods based on dedicated models [25]. On the other hand, methods based on neural networks, extended Kalman filtering, and particle filtering are not based on specific models and are usually regarded as universal approximators [25].

It is difficult to make a detailed comparison with all existing methods because the models and the methodologies associated to each method are very different. As the identification method proposed in this paper is based on a polynomial structure model, the comparative study of this section concerns methods based on similar models, i.e., the Hammerstein and Wiener models. The global advantages of the proposed method is summarized at the end of this section.

The criterion used to perform the comparison is the MSE between the regenerated output $y_r(t)$ and the output $y(t)$ of the system under test. The following two systems are identified to perform the comparison: 1) the real audio limiter previously identified in Section V-B and 2) an equivalent simulated limiter (zero-memory system). The comparison is carried out for the three signals used in Section V-B. All the methods are based on the eighth-degree polynomial model. The Wiener and Hammerstein methods are implemented using the MATLAB—System Identification Toolbox. Table I summarizes the MSE obtained for each method for both simulated and real-world system identifications.

As seen in Table I, for simulated data, the swept-sine method leads to an MSE of the same order of magnitude as the ones linked to other methods. This can be explained by the fact that all tested methods use the same polynomial structure. Moreover, the results for real-word system identification clearly shows that the swept-sine method performs better for all the tested cases.

VII. Conclusion

In this paper, a method for identification of NLSs has been presented. The result of the identification is a nonlinear model consisting of nonlinear branches, with each branch being the nth power in series with a linear filter, which is equivalent to

TABLE I
MSEs

	simulation	real-world
sine wave with $A = 1$ V		
NL convolution	0.00011	0.00023
Hammerstein	0.00014	0.0014
Wiener	0.00014	0.0015
sine wave with $A = 0.3$ V		
NL convolution	0.00026	0.00023
Hammerstein	0.00018	0.0032
Wiener	0.00018	0.0041
sawtooth signal with $A = 0.5$ V		
NL convolution	0.00054	0.00066
Hammerstein	0.00016	0.0025
Wiener	0.00017	0.0031

the generalized polynomial Hammerstein model. The method allows in particular to regenerate an output signal corresponding to any given input signal and to compare this regenerated output signal to the real-world output to validate the accuracy of the model.

The method has been applied to a real-world NLS (audio limiter). The nonlinear model has been tested for different input signals, i.e., two sine-wave signals with different levels and a sawtooth signal, and compared with other methods.

On one hand, one of the characteristics of the method is the necessity of properly designed excitation signal. For that reason, the system under test cannot be excited from a simple signal generator, but from a personal computer with an audio card, or from a signal generator with memory, in which the properly designed signal is recorded.

On the other hand, the robustness of the method has been proved regarding noise characteristics (Fig. 11) and through a real measurement test (Table I), as also presented in [16] and [17]. It has also worth noting that the method has a low calculation time cost. Compared to the methods that are not based on a specific model (e.g., extended Kalman filtering, particle filtering, or neural networks), the proposed method is straightforward with no special algorithms and, thus, easy to be implemented. In addition, the method has no need for any knowledge of the system under test.

REFERENCES

[1] T. Kailath, *Linear Systems*. Englewood Cliffs, NJ: Prentice-Hall, 1980.
[2] B. P. Lathi, *Signal Processing and Linear Systems*. Oxford, U.K.: Oxford Univ. Press, 2000.
[3] M. Schetzen, *The Volterra and Wiener Theories of Nonlinear Systems*. New York: Wiley, 1980.
[4] O. Nelles, *Nonlinear System Identification: From Classical Approaches to Neural Networks and Fuzzy Models*. Berlin, Germany: Springer-Verlag, 2001.
[5] J. S. Bendat, *Nonlinear System Techniques and Applications*. New York: Wiley, 1998.
[6] F. Thouverez and L. Jezequel, "Identification of NARMAX models on a modal base," *J. Sound Vib.*, vol. 189, no. 2, pp. 193–213, Jan. 1996.
[7] H. E. Liao and W. S. Chen, "Determination of nonlinear delay elements within NARMA models using dispersion functions," *IEEE Trans. Instrum. Meas.*, vol. 46, no. 4, pp. 868–872, Aug. 1997.
[8] Y.-W. Chen, S. Narieda, and K. Yamashita, "Blind nonlinear system identification based on a constrained hybrid genetic algorithm," *IEEE Trans. Instrum. Meas.*, vol. 52, no. 3, pp. 898–902, Jun. 2003.
[9] H. Sorenson, *Kalman Filtering: Theory and Application*. Montvale, NJ: IEEE Press, 1985.
[10] O. Cappé, S. J. Godsill, and E. Moulines, "An overview of existing methods and recent advances in sequential Monte Carlo," *Proc. IEEE*, vol. 95, no. 5, pp. 899–924, May 2007.
[11] P. Crama and J. Schoukens, "Initial estimates of Wiener and Hammerstein systems using multisine excitation," *IEEE Trans. Instrum. Meas.*, vol. 50, no. 6, pp. 1791–1795, Dec. 2001.
[12] M. Solomou, D. Rees, and N. Chiras, "Frequency domain analysis of nonlinear systems driven by multiharmonic signals," *IEEE Trans. Instrum. Meas.*, vol. 53, no. 2, pp. 243–250, Apr. 2004.
[13] E. Ceri and D. Rees, "Nonlinear distortions and multisine signals—Part 1: Measuring the best linear approximation," *IEEE Trans. Instrum. Meas.*, vol. 49, no. 3, pp. 602–609, Jun. 2000.
[14] A. H. Tan and K. Godfrey, "The generation of binary and near-binary pseudorandom signals: An overview," *IEEE Trans. Instrum. Meas.*, vol. 51, no. 4, pp. 583–588, Aug. 2002.
[15] R. Haber and L. Keviczky, *Nonlinear System Identification: Input/Output Modeling Approach*, vol. 1/2. Dordrecht, The Netherlands: Kluwer, 1999.
[16] A. Farina, "Simultaneous measurement of impulse response and distortion with a swept-sine technique," in *Proc. AES 108th Conv.*, Paris, France, Feb. 2000.
[17] E. Armelloni, A. Farina, and A. Bellini, "Non-linear convolution: A new approach for the auralization of distorting systems," in *Proc. AES 110th Conv.*, Amsterdam, The Netherlands, May 2001.
[18] L. Cohen, *Time–Frequency Analysis*. Englewood Cliffs, NJ: Prentice-Hall, 1995.
[19] P. Flandrin, *Time–Frequency/Time-Scale Analysis*. San Diego, CA: Academic, 1999.
[20] L. Cohen, "Instantaneous frequency and group delay of a filtered signal," *J. Franklin Inst.*, vol. 337, no. 4, pp. 329–346, Jul. 2000.
[21] T. Kite, "Measurement of audio equipment with log-swept sine chirps," in *Proc. AES 117th Conv.*, San Francisco, CA, Oct. 2004.
[22] W. H. Beyer, *Standard Mathematical Tables*. Boca Raton, FL: CRC Press, 1987.
[23] Y. M. Zhu, "Generalized sampling theorem," *IEEE Trans. Circuits Syst. II, Analog Digit. Signal Process.*, vol. 39, no. 8, pp. 587–588, Aug. 1992.
[24] J. Tsimbinos and K. V. Lever, "Input Nyquist sampling suffices to identify and compensate nonlinear systems," *IEEE Trans. Signal Process.*, vol. 46, no. 10, pp. 2833–2837, Oct. 1998.
[25] J. Schoukens, R. Pintelon, and Y. Rolain, "Identification of nonlinear and linear systems, similarities, differences, challenges," in *Proc. 14th IFAC Symp. Syst. Identification*, Newcastle, Australia, 2006, pp. 122–124.
[26] WWW page Dbx: Professional Products, dbx 266xl Compressor-Gate2007. [Online]. Available: http://www.dbxpro.com/266XL/266XL.php
[27] J. S. Bendat and A. G. Piersol, *Engineering Applications of Correlation and Spectral Analysis*. New York: Wiley, 1980.
[28] P. Welch, "The use of the fast Fourier transform for the estimation of power spectra," *IEEE Trans. Audio Electroacoust.*, vol. AU-15, no. 70, pp. 70–73, Jun. 1970.

Antonín Novák received the Master degree in engineering from the Czech Technical University, Prague, Czech Republic, in 2006. He is currently with the Faculty of Electrotechnical Engineering, Czech Technical University, and the Laboratoire d'Acoustique de l'Université du Maine, UMR-CNRS 6613, Le Mans, France, working toward a Ph.D. degree within the framework of the French government program, "Cotutelle de thèse."

His research interests include analysis and measurement of nonlinear systems and digital signal processing.

Laurent Simon (M'00) was born in France in 1965. He received the Ph.D. degree in acoustics from the Université du Maine, Le Mans, France, in 1994.

He is currently a Professor with the Laboratoire d'Acoustique de l'Université du Maine, UMR-CNRS 6613, Le Mans. His research interests mainly concern signal processing for acoustics and vibrations, including nonlinear system identification, inverse problems for NDT, and spectral estimation of missing data.

František Kadlec was born in Czech Republic in 1943. He received the B.S. degree in electrical engineering and the Ph.D. degree in acoustics from the Czech Technical University, Prague, Czech Republic, in 1967 and 1975, respectively.

He is currently with the Multimedia Technology Group, Radio Engineering Department, Faculty of Electrotechnical Engineering, Czech Technical University. His research interests include audio signal processing, analysis of audio systems with nonlinearities, and sound signals compression and testing from the psychoacoustic point of view.

Pierrick Lotton was born in France, in 1967. He received the Ph.D. degree in acoustics from the Université du Maine, Le Mans, France, in 1994.

He is currently a CNRS Research Fellow with the Laboratoire d'Acoustique de l'Université du Maine, UMR-CNRS 6613, Le Mans. His research interests include electroacoustic transducers and thermoacoustics.

Dr. Lotton is a member of the Audio Engineering Society and the French Acoustical Society.